



The influence of zeolite pore topology on the separation of carbon dioxide from methane

Eduardo Pérez-Botella^{a,b}, Miguel Palomino^a, Gabriel B. Báfero^c, Heloise O. Pastore^c, Susana Valencia^a, Fernando Rey^{a,*}

^a The A-Team of the Instituto de Tecnología Química, Universitat Politècnica de València-Consejo Superior de Investigaciones Científicas, Valencia 46022, Spain

^b Department of Chemical Engineering, Vrije Universiteit Brussel, Ixelles 1050, Belgium

^c Micro and Mesoporous Molecular Sieves Group, Institute of Chemistry, University of Campinas, Campinas 13083-970, Brazil

ARTICLE INFO

Keywords:

Adsorption
Carbon dioxide
Methane
Zeolites
Breakthrough
Separation

ABSTRACT

The influence of framework topology on the separation of carbon dioxide from methane has been studied in a set of small pore pure silica zeolites with CHA, IHW, ITW, LTA, MTF and RWR structures. To isolate this effect, the composition of the materials has been kept constant by using pure silica materials, which have neither aluminium in their framework nor extraframework cations that can alter the adsorption behaviour. Pure component adsorption isotherms and breakthrough experiments with synthetic mixtures resembling biogas and natural gas have been conducted. Materials Si-RWR and Si-ITW, which present channel-like topology, show higher IAST selectivities towards CO₂ due to a kinetic exclusion of methane, which in the case of Si-RWR is pore-size based and in the case of Si-ITW, topology based. High heat of adsorption of CO₂ on Si-ITW is explained through a maximisation of the dispersive interactions between the tight channels and the adsorbate. The extremely small pores of Si-RWR lead to a reduced diffusivity not only of CH₄ but also of CO₂ precluding its use as adsorbent for this separation. Si-ITW arises as a promising material in the separation of CO₂ from CH₄, having high selectivity towards CO₂ while keeping high diffusion rates and a moderate maximum capacity. A comparison of the performance of these materials with that of aluminosilicate zeolites LTA with Si/Al ratio of 5 and 13X shows that Si-ITW can be more convenient by lowering the energetic requirements of the regeneration step. Moreover, the hydrophobicity of this material can be a further advantage over traditional zeolites.

1. Introduction

Carbon dioxide is an undesired component of natural gas and biogas and needs to be removed from these mixtures in order to increase their heating value and reduce corrosion and pipe plugging problems during the treatment operations [1]. The most common separation method used in the industry at large scale facilities is aqueous amine scrubbing. This chemical absorption method is highly energy intensive, due to the nature of the process, which involves carbamate formation, as well as the need to thermally regenerate the amine solution [2]. Furthermore, corrosion of the equipment is inherent to this method, which further increases its costs [3]. Thus, alternative methods that require less energy intensive operation, such as separation by adsorption, are highly desirable, especially for small and medium scale facilities for which the capital and operating costs need to be minimised [4,5].

Zeolites have been widely applied as adsorbents for gas separation

since the breakthrough of their industrial production in the 1950s, mainly because of their uniform porosity, high thermal and chemical stability, and tuneable textural properties [6]. Among other applications, they have been proposed as adsorbents for CO₂ removal from natural gas and biogas streams. Traditional zeolites such as A-, X- or Y-type have been patented and studied as adsorbents for this separation in pressure swing adsorption (PSA) processes [7–13]. These low silica materials present high heats of adsorption of CO₂ and high thermodynamic CO₂/CH₄ selectivities, due to the interaction of the quadrupole moment of CO₂ with the extraframework cations [14]. However, the main drawbacks of these materials stem from this strong interaction as well, as it can result in inconveniently high regeneration energies, including the formation of strongly bound carbonate-like species [15], and low working capacities under pressure swing adsorption conditions [16]. Furthermore, if the natural gas or biogas stream contains moisture, which happens frequently, there will be problems with competitive

* Correspondence to: Instituto de Tecnología Química, Universitat Politècnica de València-Consejo Superior de Investigaciones Científicas, Valencia 46022, Spain.
E-mail address: frey@itq.upv.es (F. Rey).

adsorption of water and even carbonate or bicarbonate formation [17, 18].

Conversely, materials with higher Si/Al ratios, such as high- and pure silica zeolites and other compositional analogues, like aluminophosphates (AlPOs) or silicoaluminophosphates (SAPOs) present lower heats of adsorption, lower hydrophilicity, and more favourable isotherm shapes, which account for higher working capacities [16, 19–25]. As the CO₂/CH₄ selectivities on these low polarity materials are not always as high as on low silica zeolites, a compromise has to be met. Zeolites with intermediate Si/Al ratios and CO₂ heats of adsorption of 27 – 32 kJ/mol present a good compromise between selectivity and working capacity [16]. Furthermore, the pore size and topology of the material can be selected to maximise the structural selectivity. Various studies on the effect of the structure of zeolitic materials on CO₂ adsorption and on its separation from methane have shown that the interaction of CO₂ with the framework is enhanced in solids with larger framework density and close-fitting pores, where dispersion interactions are maximized via a confinement effect [20,26,27]. Other convenient separation mechanisms that have been found in new materials discovered in the last 10 years include trapdoor adsorption [28–30], guest-induced flexibility [31,32] and molecular sieving [33–35].

Following these lines, we decided to explore the separation performance of CO₂/CH₄ mixtures in pure silica materials with small pores and various pore topologies. By choosing materials with very small pore openings, we intend to exploit the molecular sieving effect and by choosing materials with close-fitting pores, we open up the possibility for a confinement effect. For this purpose, we have studied the adsorption properties of CO₂ and CH₄ on a set of small pore pure silica zeolites with CHA, IHW, ITW, LTA, MTF and RWR structures, with structural descriptors as summarized in Table 1. The materials' pore topologies have been classified as channel- or cavity-like according to visual examination of their pores. Cavity-like materials present substantial variations in the cross-sections along the pore, whereas the pore cross-section for channel-like materials presents smaller variations. Channel-like materials are thus more prone to present pores that fit closely with the adsorbate. Most of the selected structures present approximately circular pore openings with dimensions close to 4 Å. This does not apply to IHW, which has an ovoid pore opening of 3.5 × 4.3 Å, or RWR, which has an ellipsoidal pore opening of 2.8 × 5.0 Å. CHA and LTA are three-directional and possess clearly defined cavities. IHW is bidirectional and presents cavity-like pores while MTF is unidirectional

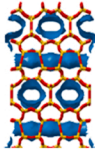
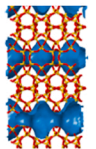
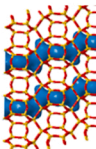
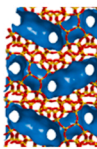
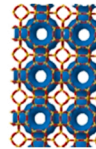
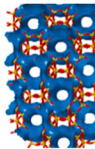
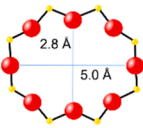
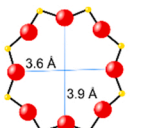
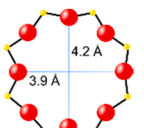
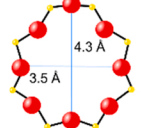
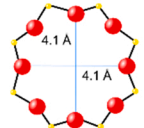
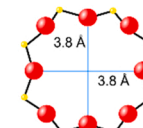
and presents cavity-like pores. RWR and ITW are both unidirectional and channel-like pores. ITW presents “side pockets”, but one of the pore dimensions remains relatively constant, which renders it channel-like from a practical perspective. We obtained a first set of results from single component adsorption isotherms, which allow for the determination of isosteric heats of adsorption and selectivities calculated using the Ideal Adsorbed Solution Theory (IAST). After that, the most promising adsorbents were selected for competitive breakthrough adsorption experiments, from which experimental selectivities and adsorbed amounts are calculated. A qualitative discussion is established by calculating purity, recovery and productivity values of a hypothetical simplified process based on the breakthrough-regeneration curve. Aluminosilicate zeolites with LTA structure and SiAl = 5 (LTA-5) and FAU structure (13X) were included in the dynamic mixture adsorption experiments for comparison.

2. Materials and methods

2.1. Synthesis

The synthesis of the different materials was done according to previously reported methods, all of them described in detail in the [supporting materials](#). Zeolite Si-MTF (MCM-35) was synthesised hydrothermally in fluoride medium using hexamethyleneimine as the structure directing agent [36]. Zeolite Si-ITW (ITQ-12) was synthesised hydrothermally in fluoride medium using 1,3,4-trimethylimidazolium hydroxide as the structure directing agent [37,38]. Zeolite Si-IHW (ITQ-32) was synthesised hydrothermally in fluoride medium using 4-cyclohexyl-1,1-dimethylpiperazinium hydroxide as the structure directing agent [39]. Zeolite Si-LTA (ITQ-29) was synthesised hydrothermally in fluoride medium using 4-methyl-2,3,6,7-tetrahydro-1 H, 5 H-pyrido[3.2.1-ij]quinolinium and tetramethylammonium hydroxides as the structure directing agents [40]. Zeolite Si-CHA (SSZ-13) was synthesised hydrothermally in fluoride medium using N,N,N-trimethyl-1-adamantammonium hydroxide as the structure directing agent [41]. Zeolite LTA-5 (UZM-9) was synthesised hydrothermally using tetraethylammonium and diethyldimethylammonium hydroxides as the structure directing agents [42]. Zeolite Si-RWR (RUB-24) was synthesised by a combined hydrothermal and topotactic conversion method [43–45]. Zeolite 13X was purchased from Aldrich.

Table 1
Structural descriptors of the small pore zeolites used in this work.

Descriptor	Si-RWR	Si-MTF	Si-ITW	Si-IHW	Si-LTA	Si-CHA
Dimensionality	1D	1D	1D	2D	3D	3D
Topology	channels	cavities	channels	cavities	cavities	cavities
View 1						
View 2						
Pore window (Å)	2.8 × 5.0	3.6 × 3.9	3.9 × 4.2	3.5 × 4.3	4.1 × 4.1	3.8 × 3.8

2.2. Characterization

The purity of the samples was checked by powder X-ray diffraction (PXRD) using a Panalytical Cubix PRO diffractometer, using Cu K α radiation ($\alpha_1 = 1.54060 \text{ \AA}$, $\alpha_2 = 1.54443 \text{ \AA}$) and a scan range from $2^\circ < 2\theta < 40^\circ$.

The amount of connectivity defects in the materials was quantified by ²⁹Si magic angle spinning nuclear magnetic resonance (MAS NMR). The spectra were recorded on a Bruker Avance III HD 400 MHz spectrometer at room temperature and $\nu_0(^{29}\text{Si}) = 79.5 \text{ MHz}$ using a spinning rate of 5 kHz with a $\pi/3$ pulse length of 3.5 μs , spinal proton decoupling and 180 s (for as-made samples) or 60 s (for calcined samples) as repetition time. The ²⁹Si chemical shift was referred to tetramethylsilane. Signals in the range of -120 to -105 ppm belong to Si(OSi)₄, whereas signals above -105 ppm belong to Si(OSi)₃(OH), i.e. silanol groups or defects [46].

Crystal size and morphology were studied by either scanning electron microscopy (SEM) using a JEOL JSM6300 microscope or field emission scanning electron microscopy (FESEM) using a ZEISS ULTRA 55 microscope.

The surface area was determined by the Brunauer-Emmet-Teller (BET) method and the micropore volume was determined by the t-plot method applied to nitrogen adsorption isotherms measured at -196 °C [47] on the volumetric device Micromeritics ASAP 2420 after degassing the samples at 400 °C under vacuum for 12 h. In some samples, determination of the micropore surface area was only possible by applying the Dubinin-Astakhov's method to CO₂ isotherms recorded at 0 °C [48]. The average pore size of some samples was obtained from adsorption isotherms of Ar at -186 °C by applying the Horvath-Kawazoe method [49].

2.3. Pure component adsorption experiments

The adsorption isotherms of CO₂ and CH₄ up to 700 kPa and at temperatures ranging from 10° to 60°C were measured on a gravimetric Hiden IGA3, and/or a volumetric Quantachrome iSorbHP. Water isotherms on Si-ITW, Si-RWR, LTA-5 and 13X were measured on a volumetric BelSorp II Max device. The CO₂ and CH₄ isotherms of 13X were obtained from literature data [12]. The binary mixture adsorption equilibria were calculated using the Ideal Adsorbed Solution Theory (IAST). First the isotherms at 25 or 30 °C were fitted to the most suitable model out of Langmuir (Si-CHA, Si-IHW, Si-ITW, Si-LTA) and Dual-Site Langmuir (Si-MTF, Si-RWR, LTA-5, 13X) and then the IAST was applied according to what is described in the literature [50,51]. The IAST selectivities were then calculated at a defined hypothetical composition (CO₂/CH₄ 20:80 or 50:50) as:

$$\alpha_{\text{CO}_2, \text{CH}_4} = \frac{x_{\text{CO}_2, \text{eq}}/y_{\text{CO}_2}}{x_{\text{CH}_4, \text{eq}}/y_{\text{CH}_4}} \quad (1)$$

Where x is the adsorbate molar fraction, the subindex eq refers to equilibrium, and y is the molar fraction of each component in the hypothetical gas phase. The isotherm measurements were linearly interpolated to obtain the isosteres and the Clausius Clapeyron equation was used for calculating the isosteric heat of adsorption q_{st} , which is the negative value of the enthalpy of adsorption on each material.

$$q_{st} = -\Delta H_{\text{ads}} = -R \left[\frac{\partial \ln P}{\partial T} \right]_Q \quad (2)$$

Where R is the ideal gas constant and T is the temperature. For the sake of accuracy, high resolution adsorption CO₂ isotherms up to 100 kPa and at temperatures ranging from 0° to 60°C were measured on a Micromeritics ASAP2010 and were used for obtaining more accurate values of the isosteric heat of adsorption at low coverages ($q_{st,0}$). A very good

overlapping was obtained between low pressure and high pressure isotherms.

2.4. Dynamic adsorption experiments

Dynamic adsorption experiments (breakthrough experiments) were conducted on a self-developed device, a scheme of which is depicted below (see Fig. 1).

In a typical experiment, a stream (25 mL STP/min) of either pure CO₂, CH₄ or mixtures thereof was passed through a bed of fresh adsorbent and the outcome of the bed was analysed with a Coriolis mass flow meter and a Hiden QGA mass spectrometer. Argon (240–272 mL/min, the exact values are presented in table S1) was used as dilution/makeup gas at the exit of the bed and helium was used as a regeneration gas. The said mixtures of CO₂ and CH₄ have compositions representative of both natural and biogas (20:80 CO₂/CH₄ and 50:50 CO₂/CH₄, respectively). A constant mass of adsorbent was used for the different samples (ca. 0.65 g). The adsorbent particle size was of 0.2–0.4 mm, and it was diluted with SiC of larger particle size (0.6–0.8 mm) to adjust the bed length properly to values between 11 and 13 cm (6.4 cm for 13 X). Internal bed diameter was 4.57 mm. These experiments were conducted at 25 °C and at pressures relevant to this separation, i.e., 200 and 700 kPa. The adsorbent was placed in the central space of a double-walled concentric column. The intermediate layer was reserved for thermal regulation using a water bath and heating was provided via an electrical mantle heater that surrounded the outer wall of the column. The pressure was kept constant using a backpressure regulator. After equilibrium is reached, the feed is switched to He (25 mL STP/min) for 20 min. Finally, still under He flow, the bed is heated to a temperature of ca. 240 °C at 10 °C/min to achieve full desorption. The regeneration temperature was consistent for each sample and in the range of 237–244 °C. More accurate control of the regeneration temperature was not possible due to the design of the column.

The breakthrough experiments data were analysed following procedures described previously, adapting them to our case [13,16,52]. The equations used to calculate the adsorbed amounts are detailed in the supplementary materials. The mixture selectivity can be obtained by applying an expression analogous to Eq. 1, where the adsorbed amounts are replaced by the ones calculated in competitive adsorption conditions.

The performance of different materials in the separation of CO₂ from CH₄ was analysed in terms of said mixture CO₂/CH₄ selectivities, adsorbent productivity and purity and recovery of both adsorbates [53]. For that purpose, the breakthrough curve is divided into three parts, which are related to a hypothetical process with three steps. The first step is adsorption, and the recovered product is methane, which is kept at a purity > 97% [25,54]. The second step is equilibration and is only considered in terms of the time it adds to the whole separation cycle. In a real PSA process, this step would be skipped and replaced by pressure equalization and/or purge steps. The third step is desorption, and the recovered product is carbon dioxide. The time needed for regeneration is taken as the time needed for the outlet concentration to go below the detection limit of CO₂ of the mass spectrometer. The productivity, recoveries and purities are calculated using the equations detailed in the SI. Due to the simplifications made and the fact that these values are fully calculated from our experimental breakthrough data, only qualitative conclusions should be drawn from these experiments. Nonetheless, the comparison with aluminosilicate materials LTA-5 (Si/Al = 5) and 13X (Si/Al = 1.2) serves to put a scale to the observations made.

3. Results and discussion

3.1. Characterization of the zeolites

The results of textural characterization, framework connectivity and crystal size and morphology can be found in Table 2. The PXRD patterns

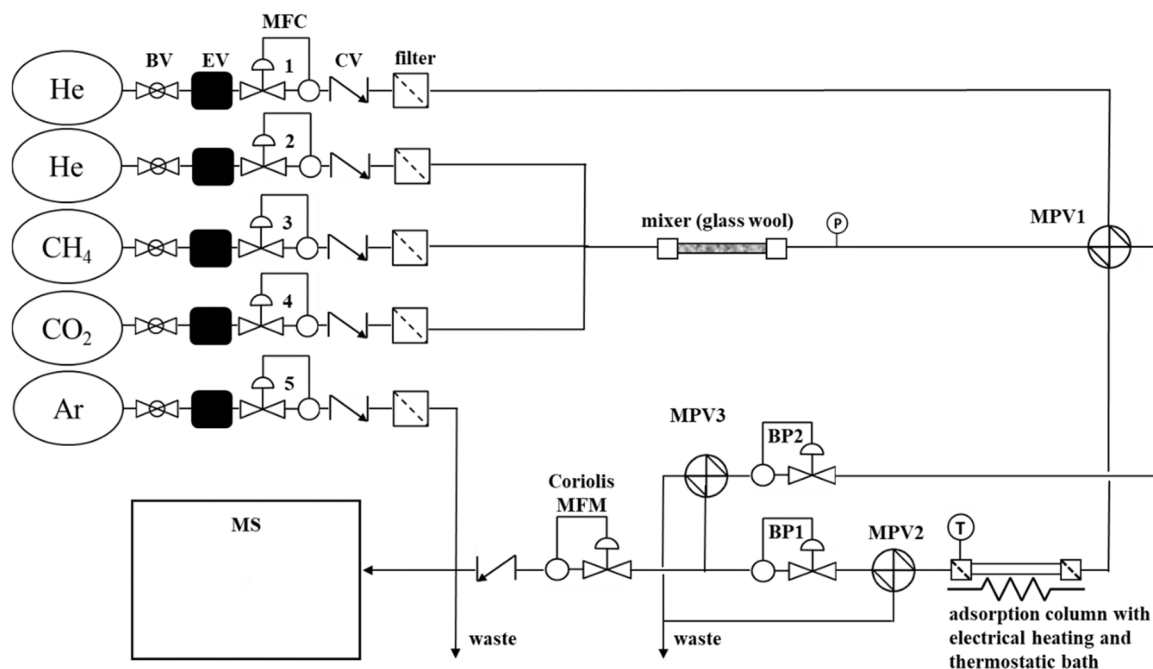


Fig. 1. Scheme of the experimental setup used for conducting competitive adsorption and separation of mixtures.

Table 2
Summary of relevant characterisation results of the studied materials.

Sample	Silanol amount (%) ^a	Crystal shape	Crystal dimensions (μm)	d_{pore} (Å) ^b	S_{BET} (m ² /g)	S_{DA} (m ² /g) ^c	V_{micro} (cm ³ /g)
Si-CHA	8	cubes	2–10	5.4	821	-	0.3
Si-IHW	0	needles	2 × 0.2 × 0.2	5.3	393	-	0.16
Si-ITW	0	indefinite	2 – 30	4.8	356	-	0.18
Si-LTA	0	cubes	0.3	6.4	811	-	0.32
Si-MTF	0	sheets	5 × 2 × 0.1	4.8	232	241	0.07
Si-RWR	1	sheets	$a \times a \times 0.1$ (1 < a < 6)	-	-	180	-
LTA-5	-	cubes	0.4	-	806	-	0.30
13X	-	-	-	-	837	-	0.31

^a The silanol amount was calculated by proper deconvolution of the ²⁹Si MAS NMR spectra [46].

^b The d_{pore} indicated here corresponds to the one determined by Horvath-Kawazoe analysis of the Ar isotherm at – 186 °C.

^c The S_{DA} refers to the surface area obtained from applying the Dubinin-Astakhov model to the CO₂ isotherm at 0 °C.

confirm the purity and crystallinity of the samples as deduced for their comparison to the patterns given for reference materials. The normalised experimental patterns are plotted together with reference patterns for comparison in Fig. 2. Reference patterns of CHA and LTA belong to low silica aluminosilicate materials, which is the reason for the different 2θ positions of the peaks compared to our experimental spectra of Si-CHA, Si-LTA, and LTA-5. The Si-RWR sample presents relatively broad peaks, which is probably due to the small crystal size (see Fig. 3).

The amount of connectivity defects in the pure silica frameworks was evaluated by proper deconvolution of the ²⁹Si MAS NMR spectrum of each sample (Fig. S6). The Si-CHA sample presents an 8% of silanol groups and the other silica materials are defect-free (see Fig. S6, Table 2).

SEM or FESEM images of the samples at adequate magnification levels are presented in Fig. 3. The highly variable particle size of the Si-ITW sample is due to repeated pelletisation and usage throughout the years. Despite of that, the sample retains the same XRD and textural properties as when it was first calcined [37], which is a clear example of the high stability of pure silica zeolites.

Textural characterization of Si-RWR was not possible using nitrogen or argon adsorption, due to important diffusional restrictions at cryogenic temperatures and thus, isotherms of CO₂ at 0 °C were measured.

Several repetitions were conducted with different equilibration conditions and on two different instruments (not shown) and the isotherm was not reproducible, probably due still to severe diffusional limitations in the 2.8 Å unidirectional channels. The value given in Table 2 is therefore only approximate, but it confirms the presence of very narrow microporosity in RWR. The characterization results of zeolite LTA-5 and the textural properties of commercial 13X sample are also presented in Table 2. The LTA, CHA and FAU materials are the ones presenting the largest BET areas and micropore volumes, which is not surprising, as they are also three-directionally connected and present large cavities. The 13X material was also examined through thermogravimetry to assess its weight loss (see Fig. S8) and compare it to the water adsorption isotherm. The weight loss was of 23%, which corresponds to a water loading of ca. 12 mmol/g, coherent with the isotherm within reasonable error.

3.2. Pure component adsorption isotherms

The complete set of CO₂ and CH₄ data for pure component adsorption isotherm at different temperatures can be found in Figs. S9-S10. The adsorption isotherms of CO₂ and CH₄ at room temperature (25 – 30 °C) are presented in Fig. 4. Again, it is not surprising that the three-

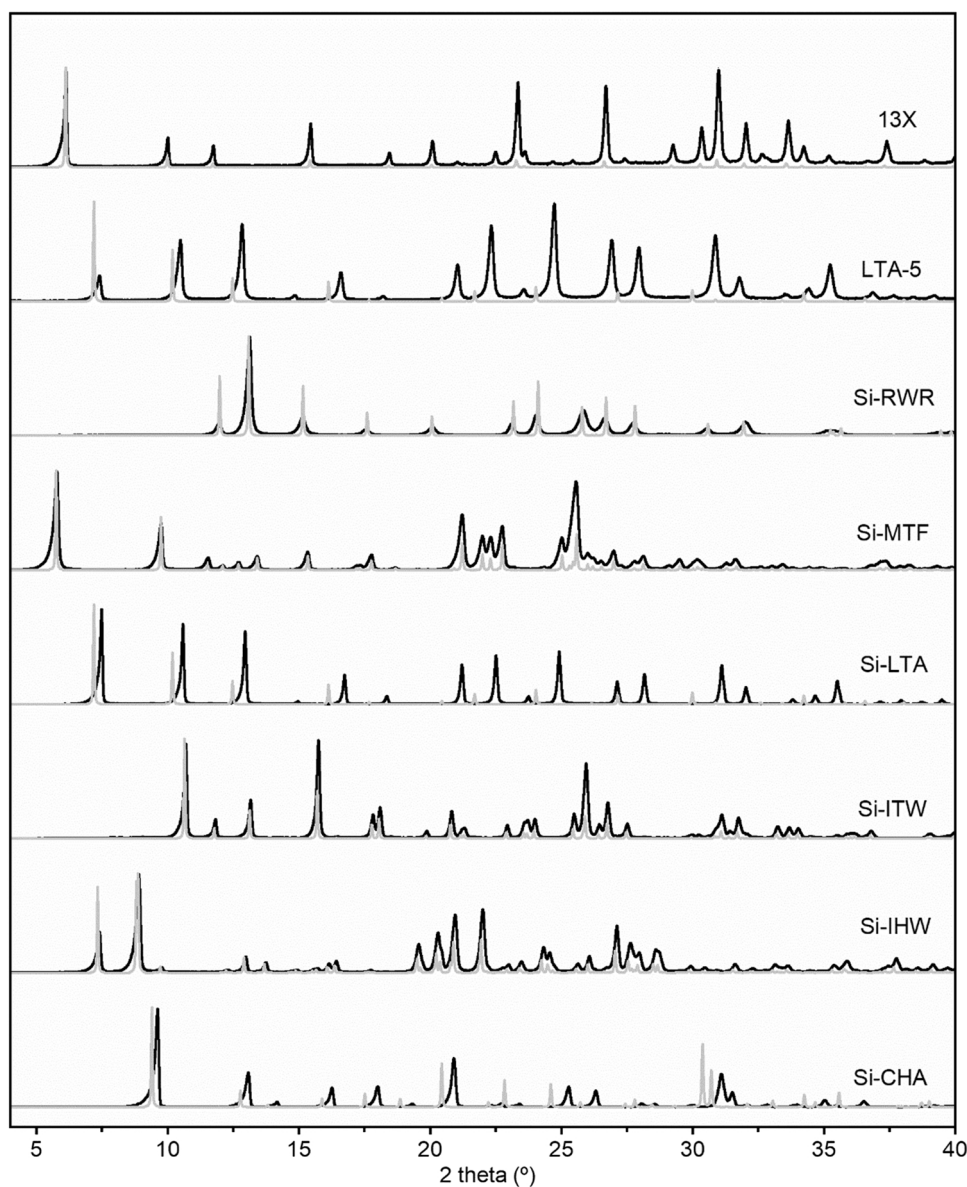


Fig. 2. X-Ray diffraction patterns of the materials used in this study. The curves in grey are from reference samples.

directional materials with cavities present the largest adsorption capacities at ambient temperature. 13X presents the largest CO₂ adsorption capacity followed by LTA-5, Si-CHA and Si-LTA. Out of these materials, Si-LTA presents a very favourable isotherm shape, which is close to linear up to 400 kPa, thus favouring a large working capacity. Si-ITW follows with a moderate CO₂ adsorption capacity and, finally, there are Si-IHW, Si-MTF and Si-RWR.

Regarding CH₄ uptakes, zeolites 13X, Si-CHA, LTA-5 and Si-LTA also present the highest adsorption capacities in the relevant range of pressures studied. They are followed by Si-IHW, Si-MTF and Si-ITW and, far below, by Si-RWR, which completely excludes CH₄ through a molecular sieving effect.

These results point towards the channel-like materials, i.e., Si-RWR and Si-ITW, presenting the highest CO₂/CH₄ selectivities. Note, however, that CO₂ presents diffusional restrictions on Si-RWR and thus, the isotherm shown is not at equilibrium. The adsorption of CH₄ is kinetically hindered also on Si-ITW, as indicated by the overlap in the isotherms measured with Hiden IGA3 and by the differences observed between isotherms measured on two devices, especially at low pressure (see Fig. S11).

The calculated IAST selectivities for hypothetical 50:50 and 20:80 CO₂/CH₄ mixtures are plotted against total pressure in Fig. 5. Si-RWR comes forward as the material possessing the largest CO₂/CH₄ selectivity. For a both mixtures, the selectivity is above 300 at all pressures. It is followed by 13X, with selectivities that decrease from ca. 100 at low pressure to 40 or 60 at 700 kPa in the cases of 50:50 or 20:80 CO₂/CH₄ mixtures, respectively. LTA-5 presents lower selectivities than 13X, starting off at 35 at low pressure but with a similar trend. Si-ITW presents relatively large selectivities at low pressure (ca. 16) that increase with pressure. In the case of the 50:50 CO₂/CH₄ mixture, it surpasses LTA-5 at 100 kPa and 13X at 400 kPa, whereas in the 20:80 CO₂/CH₄ mixture, it surpasses LTA-5 at 250 kPa and reaches similar values to 13X at 700 kPa. The selectivities on all the other pure silica materials are low throughout all the pressure range and increase slightly with pressure. The fact that Si-ITW presents pore sizes very close to those of other of the pure silica adsorbents (see Table 1) but still presents a notably higher selectivity confirms the idea that channel-like structures favour CO₂/CH₄ selectivity and that careful selection not only of the adsorbent composition or pore size, but also of its topology is relevant to a separation process.

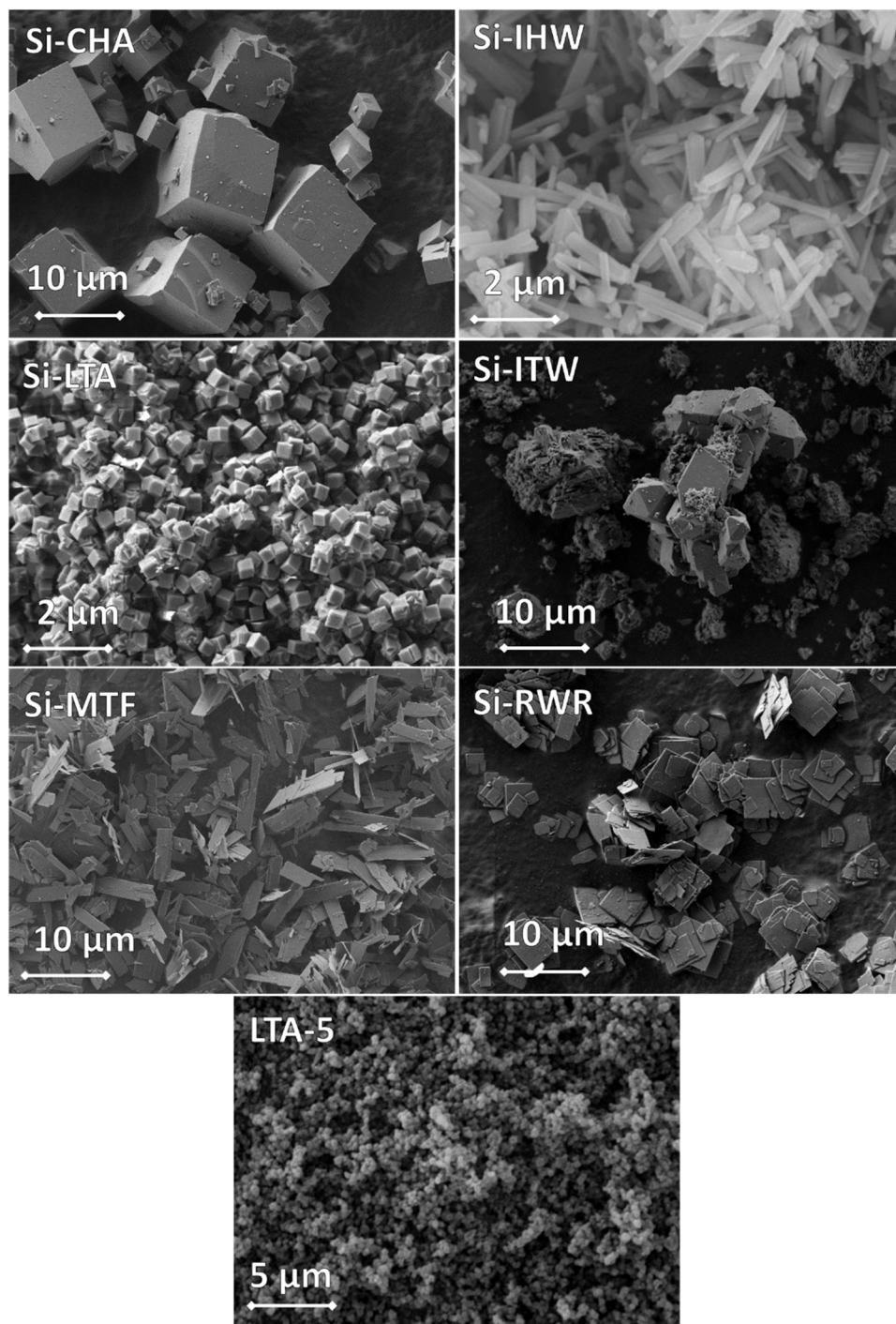


Fig. 3. FESEM and SEM images of the samples used in this study.

The isosteric heats of adsorption of CO₂ and CH₄ were calculated from the sets of equilibrated isotherms and their values at low loadings are shown in Table 3. The values for LTA-5 and 13X are taken from the works of Palomino et al. and Cavenati et al., respectively [12,19]. As can be seen, the heat of adsorption of carbon dioxide at low loading on the pure silica zeolites, is ca. 5 kJ/mol larger than that of methane, indicating a stronger interaction of the first with the zeolite surface. This interaction is based on dispersion forces. The silica zeolite presenting the largest CO₂ $q_{st,0}$ values is Si-ITW, followed by Si-MTF and Si-CHA. Enhanced interactions of CO₂ with the surface of the tight-fitting channel of Si-ITW, i.e., confinement effect, may be responsible for this relatively high value of $q_{st,0}$ [26,55,56]. This explanation may be also

valid for Si-MTF, for which the calculated mean pore size from Ar porosimetry is also very small (see Table 2). On the other hand, the relatively high CO₂ $q_{st,0}$ value of Si-CHA is probably due to dipole-quadrupole interactions between silanol groups and CO₂. In the case of 13X and LTA-5, the higher heat of adsorption at low loading comes from the interactions between the quadrupole moment of CO₂ and the charges present in the materials (cations and negatively charged framework) [26].

Finally, the water isotherms on Si-ITW, Si-RWR, LTA-5 and 13X are presented in Fig. 6. As can be seen, Si-ITW and Si-RWR are both very hydrophobic, adsorbing a negligible amount of water. The aluminosilicate zeolites 13X and LTA-5 are considerably hydrophilic and adsorb a

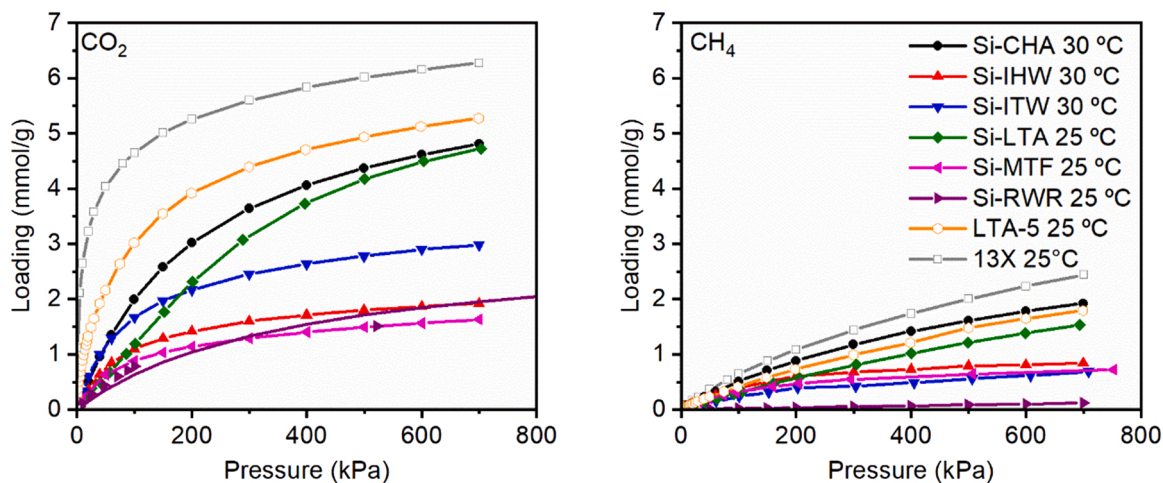


Fig. 4. Adsorption isotherms of CO₂ and CH₄ at ambient temperature on the selected pure silica and aluminosilicate zeolites. The lines are guides to the eye. The CO₂ data for RWR are not fully equilibrated. The data for 13X have been taken from Ref. [12].

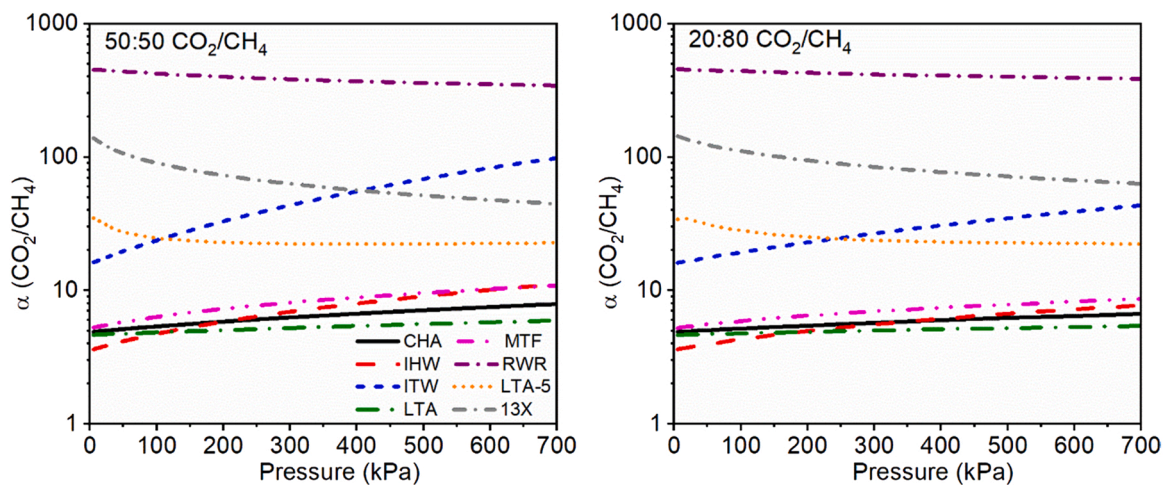


Fig. 5. CO₂/CH₄ selectivities calculated using IAST on the selected zeolites plotted against the total pressure for two relevant hypothetical compositions of biogas (50:50) and natural gas (20:80).

Table 3
Isosteric heats of adsorption at low coverage of CO₂ and CH₄ on the materials studied in this work.

Sample	$q_{st,0}$ CO ₂ (kJ/mol)	$q_{st,0}$ CH ₄ (kJ/mol)
Si-CHA	25.3	20.5
Si-IHW	22.0	15.7
Si-ITW	27.6	n.e.a
Si-LTA	22.4	15.4
Si-MTF	25.3	20.2
Si-RWR	n.e.a	n.e.a
LTA-5	32.9	17.1
13X	37.2	15.3

^a n.e. = not equilibrated

large amount of water. These results are expected, considering that defect-free pure silica zeolites, such as Si-ITW and Si-RWR, tend to be hydrophobic and the opposite applies for aluminosilicate zeolites. This is meaningful, as water adsorption usually decreases the efficiency of the separation of CO₂ by competition and by making the regeneration step more difficult [17,18].

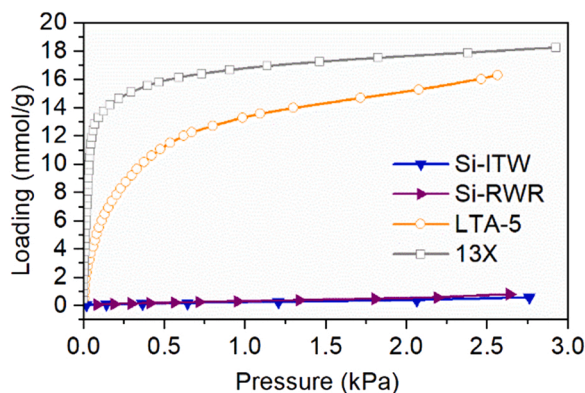


Fig. 6. Water adsorption isotherms on Si-ITW, Si-RWR, LTA-5 and 13X at 25 °C.

3.3. Dynamic breakthrough adsorption experiments

The materials presenting the highest ideal CO₂/CH₄ selectivities, i.e., Si-RWR, Si-ITW, Si-LTA, LTA-5 and 13X were further studied by carrying

out breakthrough adsorption experiments of pure components and of CO₂/CH₄ mixtures in 1:1 (simulating biogas) and 1:4 (simulating natural gas) molar ratios (see Table 4). The composition and corresponding flow rates for each experiment are presented in Table 4.

Exact amounts of pelletised and sieved material and bed heights are detailed in Table 5.

Single component breakthrough experiments at 200 kPa were carried out on Si-LTA, LTA-5, Si-ITW and Si-RWR. The adsorbed amounts obtained from these experiments are compared to the adsorbed amounts obtained from the isotherms in Fig. 7. As can be seen, the adsorbed amounts calculated from the breakthrough experiments match qualitatively well with the adsorption isotherms. In most cases, these are above the loadings given by the isotherm and the deviation is larger for CH₄ than for CO₂. This analysis is important to contextualize the results and the conclusions to be drawn also from the mixture breakthrough experiments. The amounts adsorbed calculated in the mixture experiments will be subject to considerable relative error, especially for CH₄, which is the least strongly adsorbed component [57]. Nevertheless, it will allow us to compare between the different materials in terms of their performance, especially since the conditions have been kept constant throughout this study.

Figs. 8 and 9 show the breakthrough curves at 200 and 700 kPa of CO₂/CH₄ mixtures (50:50 and 20:80, respectively) on Si-LTA, LTA-5, Si-ITW, Si-RWR and 13X. Normalized flows ($\dot{n}_i/\dot{n}_{i,0}$), defined as the outgoing flow divided by the feed flow of a single component, are plotted against time. Visual examination of the plots already allows to obtain of key qualitative conclusions. As can be seen, despite of competition between the adsorbates, in all the experiments CH₄ is the least and less strongly adsorbed component of the mixture and therefore breaks through in the first place. The displacement of methane by the more strongly adsorbed carbon dioxide is seen as a roll-up, in which the flow of methane coming out of the column is higher than that in the feed ($\dot{n}_i/\dot{n}_{i,0} > 1$) until CO₂ breaks through, especially notorious for the 50:50 mixture. Another general feature of these breakthrough profiles is that, before the breakthrough of CH₄, the total flow coming out of the column (consisting purely of He at early times) decreases temporarily. This is because a substantial part of the incoming CO₂/CH₄ feed is being adsorbed. For a certain composition, increasing the pressure of the process from 200 to 700 kPa increases the adsorption capacity and thus, the duration of the adsorption step. Lower concentration of CO₂ also leads to a longer adsorption step.

In this competitive adsorption step, the desired product is methane, which is the product ideally recovered at the exit of the column. The difference in breakthrough times of both adsorbates is therefore a measure of the performance of the different materials. The upper limit in adsorbent productivity is also given by the difference in the breakthrough times and thus, longer times will contribute to a larger methane productivity, higher adsorbed amount of CO₂ and overall, more favourable process economics, as the size of the bed and the adsorbent inventory can be reduced. Qualitatively, the separation performance of the studied materials for all four studied conditions follows the trend 13X > > LTA-5 > Si-ITW > Si-LTA > > Si-RWR.

Zeolite 13X is the adsorbent presenting the largest difference between breakthrough times of both components, distantly followed by LTA-5. The superiority of 13X is based on its large adsorption capacity for CO₂ and, especially at the lower pressure, its superior affinity towards CO₂ under competitive conditions. This higher affinity results in a

Table 4
Feed compositions used for the breakthrough experiments.

Feed	y_{CO_2}	y_{CH_4}	V_{CO_2} (mL STP/min)	V_{CH_4} (mL STP/min)
CO ₂	1	0	25	0
CH ₄	0	1	0	25
CO ₂ /CH ₄ 1:4	0.2	0.8	5	20
CO ₂ /CH ₄ 1:1	0.5	0.5	12.5	12.5

Table 5
Mass of adsorbents and bed length used for the breakthrough experiments.

Material	m (g)	l_b (cm)
Si-ITW	0.6652	12.5
Si-LTA	0.6535	12.9
Si-RWR	0.6550	11.7
LTA-5	0.6618	12.5
13X	0.6530	6.4 ^a

^a This different bed length is expected to have an impact only on the axial dispersion, which could affect the breakthrough curve shape, but the equilibrium data will not be affected.

substantially higher mixture selectivity, especially at lower CO₂ concentrations (see Table 6), in qualitative coherence with the IAST prediction (Fig. 5). LTA-5 behaves similarly, but the time frame in which pure methane exits the column is drastically reduced, which indicates a lower productivity limit in a hypothetical process. The reason for this poorer performance lies in its lower CO₂ adsorption capacity. Considering the pure-silica materials, Si-ITW separates both components better than Si-LTA under most conditions, due to the larger CO₂/CH₄ selectivity derived from enhanced interactions with CO₂ in its close-fitting pores. Nevertheless, the breakthrough of CO₂ is less steep than on the other materials, probably due to the kinetic limitations of CH₄. Si-LTA separates these gases, but only appears to be competitive to Si-ITW and the aluminosilicate materials at high concentrations of CO₂ and high pressures. Si-RWR barely separates these gases despite its high CO₂/CH₄ IAST selectivity, mainly due to its low adsorption capacities, but also due to reduced diffusion of CO₂. The kinetic hindrances that CO₂ encounters on this material are observed as well as a slow rise to the final concentration, especially at higher pressure.

In the case of the biogas-like mixture (CO₂/CH₄ 50:50) at 700 kPa (Fig. 8), the performance of pure silica materials Si-LTA and Si-ITW is comparable to that of LTA-5 and also roughly to that of 13X. The adsorption capacity of the pure silica materials increases more steeply with pressure above 200 kPa, whereas the isotherm of the aluminosilicate zeolites is already reaching their plateau. In the case of the natural gas-like mixture (CO₂/CH₄ 20:80) (Fig. 9), zeolite 13X is by far superior to the other materials, but zeolites LTA-5 and Si-ITW behave similarly, especially at 700 kPa. From these results, we can state that depending on the specific process conditions, several types of zeolitic materials may be more convenient than others. From the point of view of the adsorption step, the performance of pure silica zeolites is improved at high partial pressures of CO₂ and these materials become competitive with aluminosilicate zeolites at CO₂ partial pressures > 350 kPa. Zeolite 13X remains unbeaten for applications in which low concentrations of CO₂ are expected, especially at low total pressure.

3.4. Regeneration experiments

The separation process has a final step, the regeneration of the adsorbent, which is typically carried out by decreasing the pressure of the system, by increasing the temperature or by combining both. Regeneration profiles were measured at the end of each of the previous adsorption experiments and are shown in Figs. 10 and 11 for the CO₂/CH₄ 50:50 and 20:80 mixtures, respectively. In a typical regeneration experiment, the feed was switched to pure He, the total molar flow rate was kept constant, and pressure oscillations due to changes in valve positions were minimised by proper operation of the system. The normalised molar flows of CO₂ and CH₄ are referred to the feed in the adsorption step, whereas the He normalised flow is referred to the nominal flow in this step. After 20 min of isothermal He flow, the temperature in the bed was increased to > 200 °C using an external resistive heater. In this step, the component to be recovered is carbon dioxide, especially if the methane upgrading process is coupled to carbon dioxide capture. By means of a combined analysis of the adsorption and desorption steps, the performance of the different materials can be

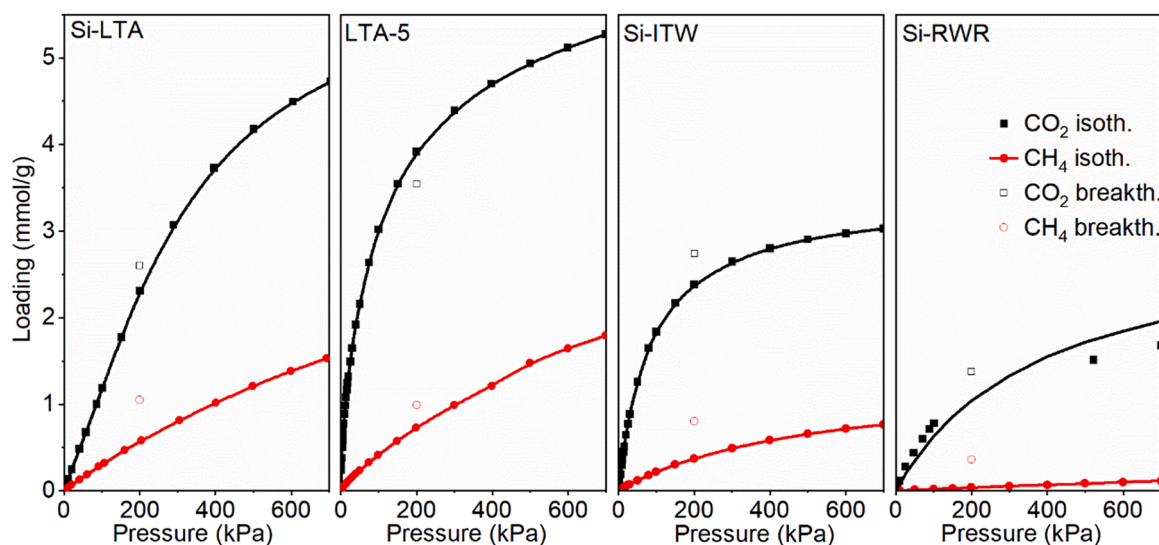


Fig. 7. Adsorption isotherms of CO₂ and CH₄ on Si-LTA, LTA-5, Si-ITW and Si-RWR at 25 °C compared with the amounts adsorbed calculated from pure component breakthrough adsorption experiments. Lines are guides to the eye. The ITW isotherm at 25 °C was estimated from the 20 °C and 30 °C isotherms as explained in the SI (Fig. S12).

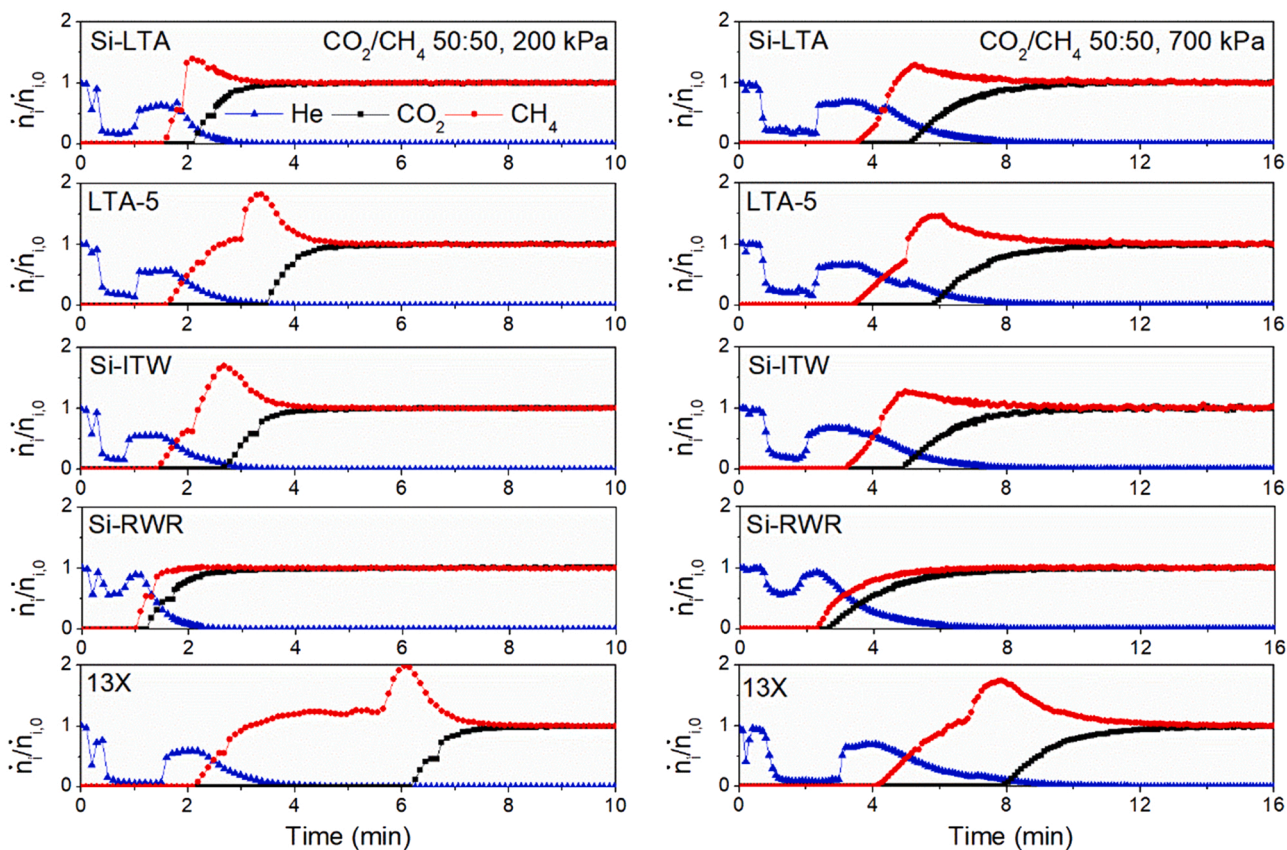


Fig. 8. Breakthrough curves of the CO₂/CH₄ 50:50 mixture at 200 kPa (left) and 700 kPa (right) on Si-LTA, LTA-5, Si-ITW, Si-RWR and 13X.

thoroughly analysed considering all the relevant parameters, such as productivity, recovery, purity and energy required for the regeneration step. These results are calculated as described in the SI and presented in Table 6.

As can be deduced from the regeneration profiles, complete regeneration is far more energy intensive on 13X than on the other materials. In Table 6, it is shown that important amounts of CO₂ are released from this material once the temperature starts increasing (38–52%) and high

temperatures (80–100 °C) are required for the concentration of CO₂ to fall below the detection limit of the mass spectrometer. LTA-5 also requires an increase in the temperature for full desorption, but the amount desorbed upon this input of thermal energy is very small in the experiments carried out at 200 kPa. At higher operation pressures, the regeneration of this material requires temperatures of ca. 80 °C, otherwise ca. 10% of the CO₂ is not desorbed. Si-RWR surprisingly also presents small desorption peaks upon heating up to (40 – 60 °C). Again,

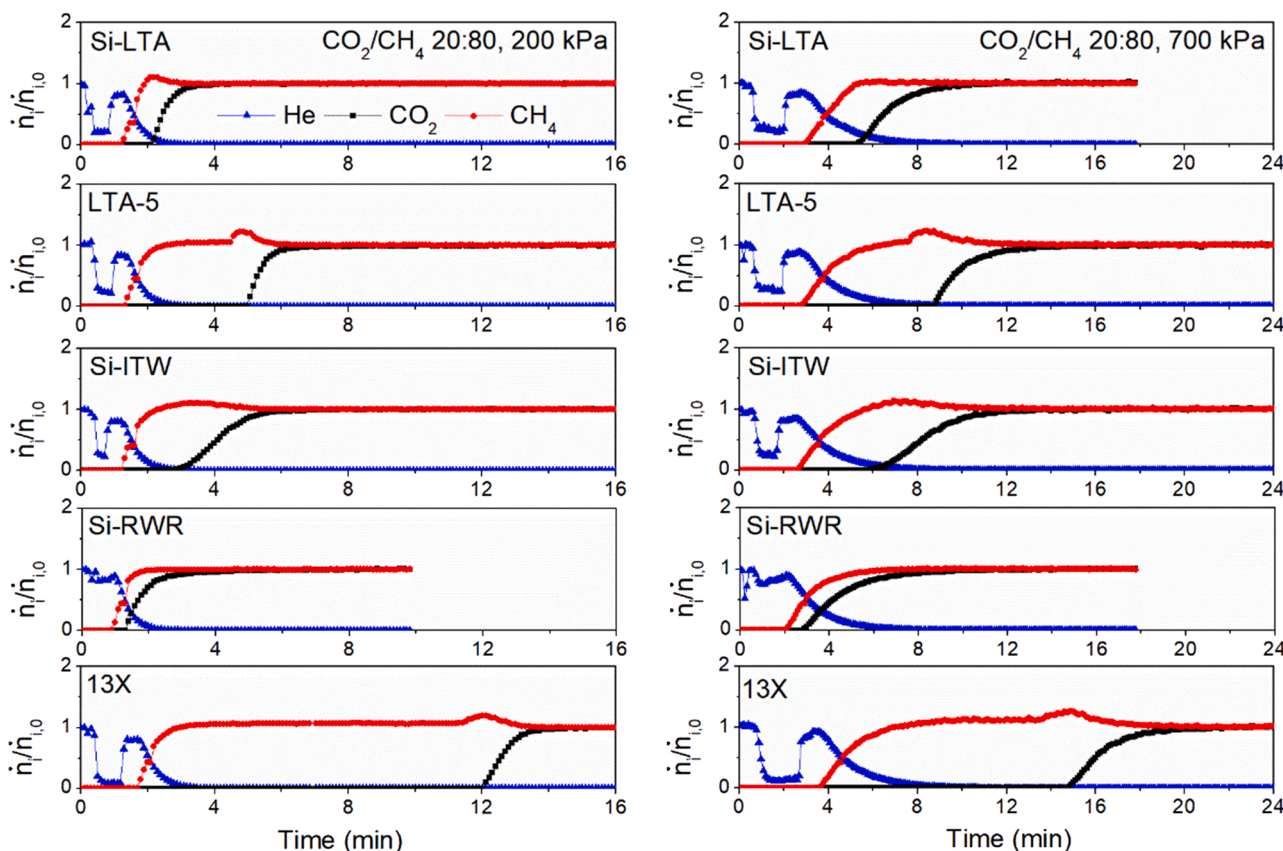


Fig. 9. Breakthrough curves of the CO₂/CH₄ 20:80 mixture at 200 kPa (left) and 700 kPa (right) on Si-LTA, LTA-5, Si-ITW, Si-RWR and 13X.

Table 6

Results obtained from the CO₂/CH₄ mixture breakthrough adsorption experiments and relevant process parameters.

Condition	Material	Q _{CO2}	Q _{CH4}	α _{real}	Productivity (mol/kg/h)	CH ₄ recovery	CO ₂ purity	CO ₂ recovery	t _{reg} (min)	Thermal desorption (%)	T _{max} (°C)
CO ₂ /CH ₄ 50:50 200 kPa	Si-LTA	1.34	0.47	2.9	2.81	47%	74%	99%	5.5	0%	25
	LTA-5	2.46	0.35	7.1	4.29	84%	88%	99%	20	0.8%	58
	Si-ITW	1.81	0.24	7.5	5.26	82%	88%	99%	8.9	0%	25
	Si-RWR	0.72	0.25	2.9	0.13	16%	74%	100%	20	1.8%	49
	13X	4.37	0.13	33.6	33.0	97%	97%	97%	20	39%	81
CO ₂ /CH ₄ 50:50 700 kPa	Si-LTA	3.04	0.63	4.8	3.33	65%	83%	99%	12.1	0%	25
	LTA-5	3.73	0.45	8.33	3.88	81%	89%	99%	20	9.4%	80
	Si-ITW	2.78	0.40	6.9	2.59	76%	87%	99%	20	0.11%	30
	Si-RWR	1.20	0.45	2.7	0.13	12%	73%	100%	20	7.8%	63
	13X	6.52	1.93	3.3	6.97	66%	77%	98%	20	38%	100
CO ₂ /CH ₄ 20:80 200 kPa	Si-LTA	0.51	0.77	2.7	7.65	63%	40%	94%	6.6	0%	25
	LTA-5	1.49	0.63	9.5	13.43	90%	70%	90%	20	1.1%	58
	Si-ITW	1.06	0.57	7.5	15.45	86%	65%	91%	8.5	0%	25
	Si-RWR	0.29	0.41	2.9	1.77	47%	42%	97%	6.9	0%	25
	13X	3.57	0.30	47.5	28.29	98%	88%	91%	20	46%	81
CO ₂ /CH ₄ 20:80 700 kPa	Si-LTA	2.21	4.53	1.9	11.33	43%	33%	95%	11.5	0%	25
	LTA-5	2.33	0.90	10.4	16.78	91%	72%	89%	20	11%	74
	Si-ITW	1.84	0.67	10.9	12.05	90%	73%	90%	20	0.08%	27
	Si-RWR	0.49	0.53	3.7	1.15	55%	48%	96%	20	4.8%	57
	13X	4.81	4.39	4.4	27.32	80%	90%	52%	20	52%	103

*Methane purities in product 1 are fixed at > 97%, according to natural gas specifications [54].

only at higher pressures is the amount of CO₂ thermally desorbed significant (5 – 8%). Si-ITW is fully regenerated in 8 – 9 min under He flow without the need of increasing the temperature in cases where the adsorption step was conducted at 200 kPa. At 700 kPa, reaching 30 °C is enough to ensure full desorption, though the amount desorbed through heating is very small (ca. 0.1%). Si-LTA is fully regenerated in all cases with just the action of the purge gas. The large cavities and the 3D-connected pores of this purely siliceous material ensure a very fast and

efficient regeneration just by flowing He, which in truth just lowers the partial pressure of the adsorptives, as it is not adsorbed. At 200 kPa, periods of 5–7 min are necessary while at 700 kPa, ca. 12 min are needed for full desorption. Increasing the pressure increases the regeneration time of all the adsorbents and the temperatures needed for complete regeneration in Si-RWR, Si-ITW, LTA-5 and 13X.

Regarding the experimental CO₂/CH₄ selectivities, the materials that stand out are 13X at low pressure (30 – 50), and LTA-5 and Si-ITW,

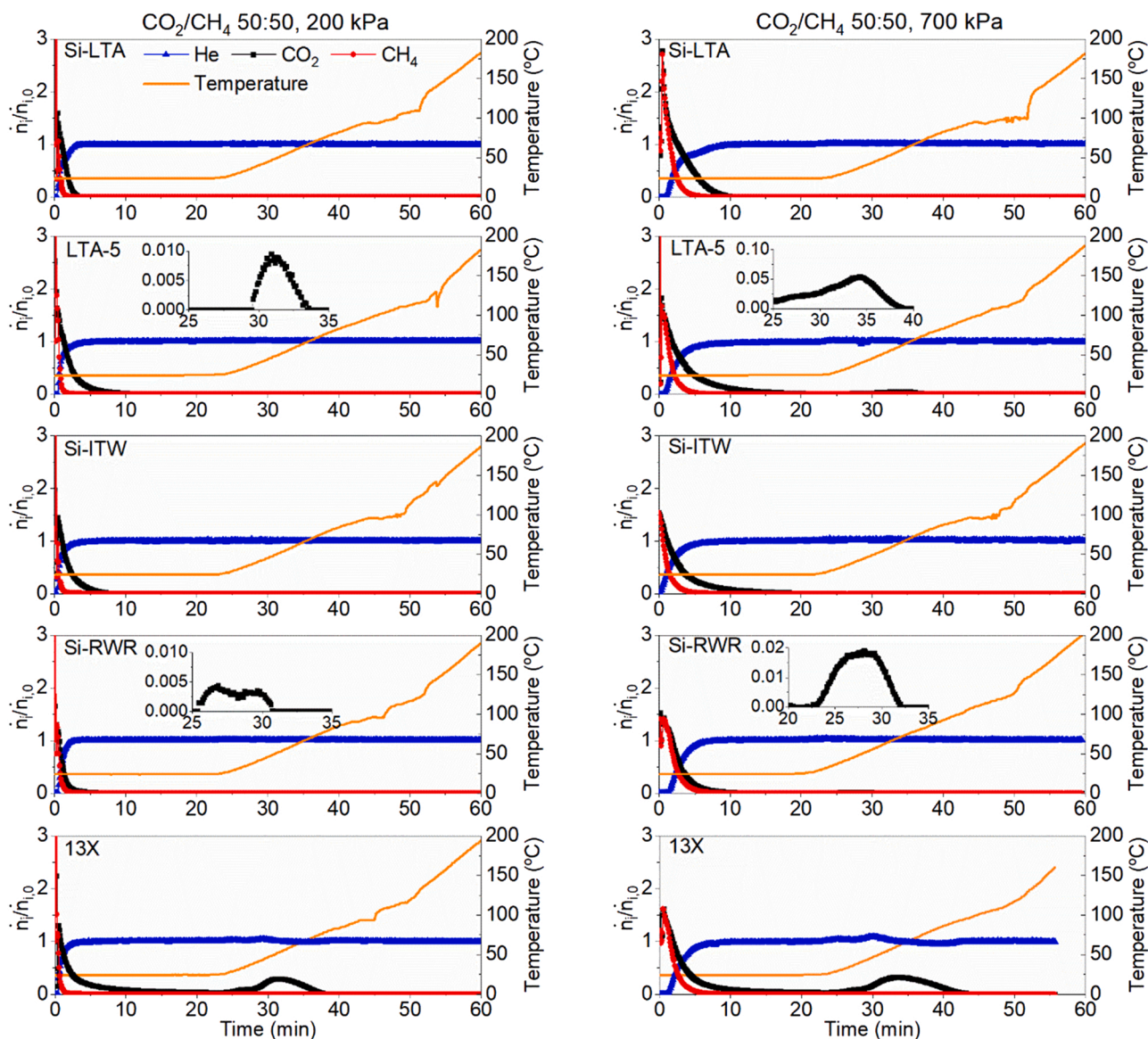


Fig. 10. Regeneration profiles of the CO₂/CH₄ 50:50 mixture at 200 kPa (left) and 700 kPa (right) on Si-LTA, LTA-5, Si-ITW, Si-RWR and 13X. Insets depict zoomed-in CO₂ desorption peaks.

which present similar and moderately high real selectivities (7 – 10) in all cases. Interestingly, the real selectivities are lower than the IAST selectivities on all materials, and they do not evolve with pressure in the same manner. In terms of productivity, zeolite 13X surpasses LTA-5 and Si-ITW by a factor of 2 in most cases, except in the 20:80 mixture at 200 kPa, where it is superior by a factor of 6. Its recoveries and purities are very high at low pressure, but at higher pressure, the amount of methane that remains adsorbed lowers the overall CH₄ recovery and the CO₂ purity. This notable increase in the amount of methane adsorbed at higher pressure changes the situation completely and limits the applicability of 13X to cases in which the partial pressure of methane is below 350 kPa. Under these circumstances, the chemical potential for adsorption of methane overpowers the strong quadrupole-dipole interactions between CO₂ and the charged framework. LTA-5 and Si-ITW present similar performances, with Si-ITW being slightly better than LTA-5 at lower pressure and vice versa. The reason for this small but consistent advantage lays in the shorter regeneration time for Si-ITW at lower pressure, which stems from its lower CO₂ heat of adsorption. The higher adsorption capacity of LTA-5 also plays a role in its larger productivity at high pressure. Their recoveries and purities are similar in all

cases. Si-LTA operates reasonably well at high CO₂ partial pressure, i.e., in the separation of the 50:50 mixture at 700 kPa, but rather poorly in all other conditions. Productivities on this material are moderate to high, partly due to the easy regeneration that allows for reducing the total cycle duration, but the recoveries and purities achieved are not promising in most situations. Si-RWR cannot be applied for the separation of CO₂ from CH₄ at any of the studied conditions. The productivity on this material is the lowest out of the ones studied and furthermore, its regeneration is not easy, due to the kinetic restrictions mentioned above. Its low adsorption capacity is also a limiting factor.

Overall, 13X presents the most advantageous properties in terms of the mass balance. Despite the lower CH₄ recoveries and CO₂ purities at higher pressure, if the desired product is methane, it gives the highest productivities. If a simultaneous CO₂ capture is intended, this material is not recommended at high pressure. In any case, a substantial amount (38 – 53%) of CO₂ is desorbed from this material only after heating at 80 – 100 °C, which means that an important energy penalty is inherent to the use of this material. It will also need a longer cycle time, since heating and cooling of the separation unit will be required. This important drawback makes other adsorbents competitive, especially for

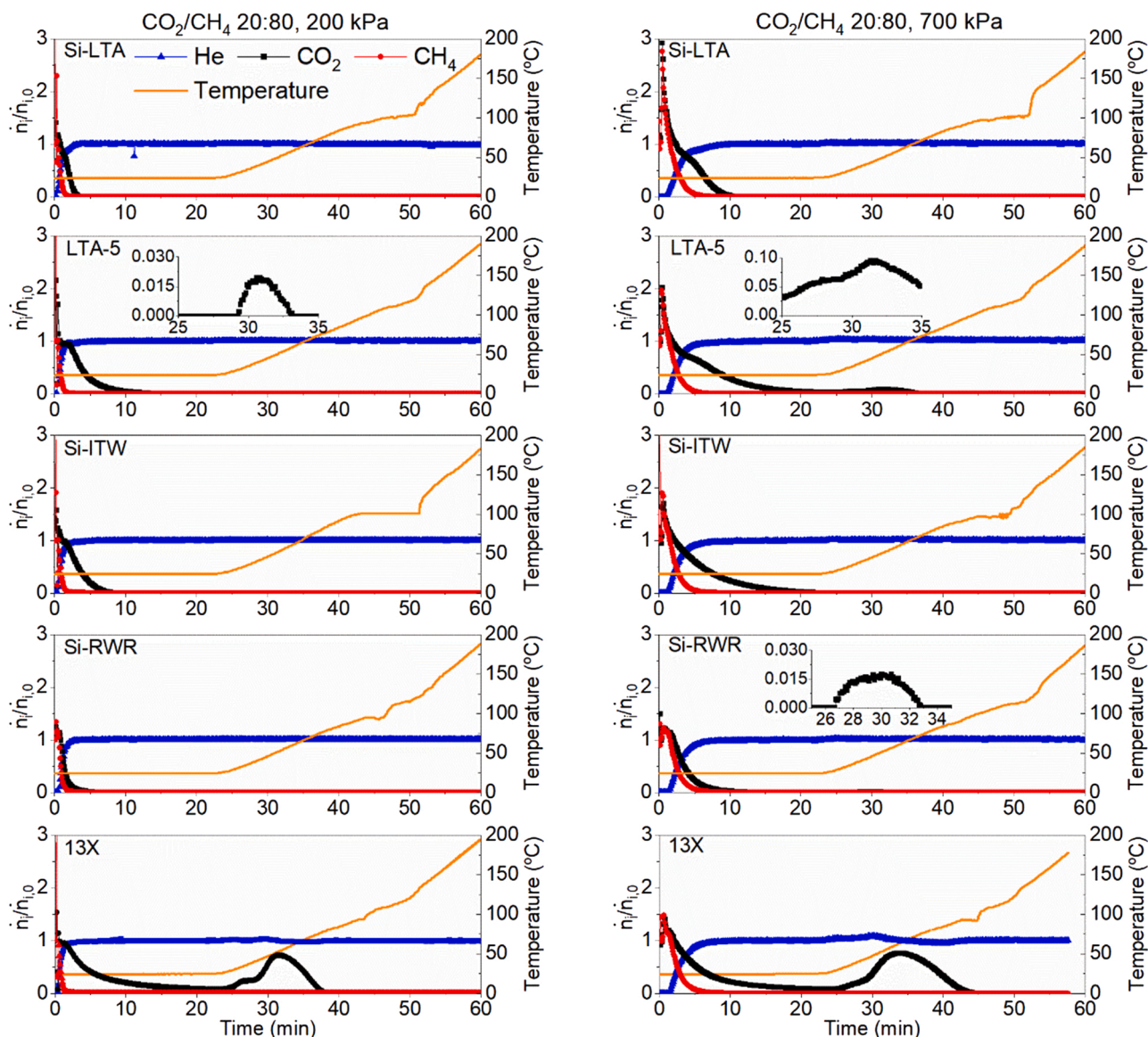


Fig. 11. Regeneration profiles of the CO₂/CH₄ 20:80 mixture at 200 kPa (left) and 700 kPa (right) on Si-LTA, LTA-5, Si-ITW, Si-RWR and 13X. Insets depict zoomed-in CO₂ desorption peaks.

separating streams with higher partial pressure of CO₂. LTA-5 and Si-ITW present similar performances, with high productivities, recoveries, and purities in most cases. According to said parameters, LTA-5 is a slightly better adsorbent at higher pressure, while Si-ITW stands out at lower pressure. Nevertheless, if the energy required for regeneration is considered, Si-ITW offers a very consistent regenerability by only needing a purge gas (lowering of partial pressure) to desorb > 99.8% of CO₂ in all cases, whereas LTA-5 needs an increase in temperature to 80 °C to desorb 10% of the CO₂ in the experiments where the adsorption was carried out at high pressure. The desorption in the pure silica materials is fast and complete by only lowering the partial pressure of CO₂, and in a real process this could make an adsorbent with moderately high selectivity and adsorption capacity like Si-ITW more advantageous than aluminosilicate zeolites. Furthermore, the effect of moisture present in real mixtures can be devastating for the performance of aluminosilicate materials (see Fig. 6), lowering their capacity, and making their regeneration even more energy intensive. Otherwise, a previous drying step should be added, with the additional costs, whereas a process implementing a hydrophobic adsorbent for the separation of CO₂ from CH₄, could rely on a simple condensation step to remove the water present in

the feed or even in the methane product.

A further and very important drawback that needs to be overcome for the use of Si-ITW, and in general, other custom materials, to be really applicable to a real separation process is their expensive and environmentally unfriendly synthesis procedure. In this work, the synthesis was carried out via the original procedure described by Boix et al. using a non-commercial organic structure directing agent [37,38]. Nevertheless, more recently the synthesis of this material using more benign conditions has been patented and is still subject of further research, the driving force being the very promising properties of this material for adsorption and catalysis [58,59].

4. Conclusions

Pure silica small pore zeolites with various structural and topological features have been studied for their applicability to the separation of CO₂ from CH₄. This selection includes widely reported Si-LTA and Si-CHA, with large cavities and tridirectionally connected pores, Si-IHW, with cavities and a bidirectional pore system, Si-MTF, also cavity-like but unidirectional and the channel-like unidirectional materials Si-

ITW and Si-RWR. A comparison with reference aluminosilicate materials LTA-5 and 13X has been established. Out of the studied pure silica materials, the channel-like small pore material Si-ITW presents the best features to be applied as an adsorbent for the separation of CO₂ from CH₄ in a pressure swing adsorption process, with performance parameters similar to LTA-5, but improved regenerability. The high selectivity in this material bases on improved interactions between CO₂ and the material's close-fitting pores, as well as on a kinetic exclusion of CH₄. Contrarily, the other channel-like material, i.e., Si-RWR, presented remarkably high IAST selectivities, but performs poorly in the real separation, due to kinetic restrictions of CO₂ and low adsorption capacity, both features probably stemming from its very narrow pores. The lower polarity materials will not be of practical applicability in the short term due to scale-up limitations in their production, but in the long term they may be more promising than benchmark materials, such as 13X, under certain conditions. It seems unlikely that pure and high-silica zeolites will perform better than 13X at partial pressures of CO₂ < 100 kPa. Nevertheless, in natural gas and biogas sources that contain a high amount of CO₂ (and water), the lower polarity materials may become competitors of the well-established aluminosilicate zeolites given that a suitable synthesis procedure is developed.

There is another important conclusion drawn from this work. Pure component isotherms on their own may be misleading in the search for a suitable adsorbent for a separation process. By measuring adsorption kinetics, as well, more firm conjectures can be made. It is, however, breakthrough experiments conducted at relevant process conditions that give a realistic outlook on the applicability of an adsorbent to a certain adsorption process. In breakthrough experiments, the interplay between kinetics and thermodynamics can be observed and extrapolated to a real separation.

CRedit authorship contribution statement

Eduardo Pérez-Botella: Investigation, Formal analysis, Methodology, Writing – original draft. **Miguel Palomino:** Investigation, Formal analysis, Writing – review & editing. **Gabriel B. Báfero:** Investigation, Resources, Writing – review & editing. **Heloise O. Pastore:** Resources, Supervision, Writing – review & editing. **Susana Valencia:** Resources, Supervision, Writing – review & editing. **Fernando Rey:** Project administration, Supervision, Writing – review & editing.

Declaration of Competing Interest

The authors declare that they have no known competing financial interests or personal relationships that could have appeared to influence the work reported in this paper.

Data Availability

Data will be made available on request.

Acknowledgements

Financial support by the Spanish Ministry of Science and Innovation (CEX2021-001230-S grant funded by MCIN/AEI/10.13039/501100011033 and TED2021-130191B-C41 grant funded by MCIN/AEI/10.13039/501100011033 and by “ERDF A way of making Europe” by the European Union NextGenerationEU/PRTR) are gratefully acknowledged. E.P-B., M.P., F.R. and S.V. thank the financial support by the Generalitat Valenciana (Prometeo 2021/077). This study forms part of the Advanced Materials programme and was supported by MCIN with partial funding from European Union Next Generation EU (PRTR-C17. I1) and by Generalitat Valenciana (MFA/2022/047). E.P-B. acknowledges the Spanish Ministry of Education and Professional Training for the grant FPU15/01602. H.O.P. and G.B.B. acknowledge the Conselho Nacional de Pesquisa Científica e Tecnológica (CNPq – 140849/2020–3,

G.B.B. scholarship). The Microscopy Service of the UPV is acknowledged for their help in sample characterisation.

Supplemental files

Supplementary information (SI): Synthesis procedures, additional characterisation, and adsorption results. Explanation of breakthrough data analysis.

Appendix A. Supporting information

Supplementary data associated with this article can be found in the online version at [doi:10.1016/j.jcou.2023.102490](https://doi.org/10.1016/j.jcou.2023.102490).

references

- [1] M. Tagliabue, D. Farrusseng, S. Valencia, S. Aguado, U. Ravon, C. Rizzo, A. Corma, C. Mirodatos, Natural gas treating by selective adsorption: material science and chemical engineering interplay, *Chem. Eng. J.* 155 (2009) 553–566, <https://doi.org/10.1016/j.ccej.2009.09.010>.
- [2] A.J. Kidnay, W.R. Parrish, *Fundamentals of Natural Gas Processing*, Taylor & Francis Group, 2006, <https://doi.org/10.1201/9781420014044>.
- [3] T.E. Rufford, S. Smart, G.C.Y. Watson, B.F. Graham, J. Boxall, J.C. Diniz da Costa, E.F. May, The removal of CO₂ and N₂ from natural gas: a review of conventional and emerging process technologies, *J. Pet. Sci. Eng.* 94–95 (2012) 123–154, <https://doi.org/10.1016/j.petrol.2012.06.016>.
- [4] D.S. Sholl, R.P. Lively, Seven chemical separations to change the world, *Nature* 532 (2016) 435–437, <https://doi.org/10.1038/532435a>.
- [5] M. Bui, C.S. Adjiman, A. Bardow, E.J. Anthony, A. Boston, S. Brown, P.S. Fennell, S. Fuss, A. Galindo, L.A. Hackett, J.P. Hallett, H.J. Herzog, G. Jackson, J. Kemper, S. Krevor, G.C. Maitland, M. Matuszewski, I.S. Metcalfe, C. Petit, G. Puxty, J. Reimer, D.M. Reiner, E.S. Rubin, S.A. Scott, N. Shah, B. Smit, J.P.M. Trusler, P. Webley, J. Wilcox, N. Mac Dowell, Carbon capture and storage (CCS): the way forward, *Energy Environ. Sci.* 11 (2018) 1062–1176, <https://doi.org/10.1039/c7ee02342a>.
- [6] E. Pérez-Botella, S. Valencia, F. Rey, Zeolites in adsorption processes: state of the art and future prospects, *Chem. Rev.* (2022), <https://doi.org/10.1021/acs.chemrev.2c00140>.
- [7] J.J. Collins, Bulk separation of carbon dioxide from natural gas, US Patent 3,751,878, 1973.
- [8] S. Sircar, R. Kumar, W.R. Koch, J. VanSloun, Recovery of methane from land fill gas., US 4770676, 1988.
- [9] R. Kumar, Adsorptive process for producing two gas streams from a gas mixture, US Patent 5026406, 1991.
- [10] S.J. Chen, Y. Fu, Y.X. Huang, Z.C. Tao, M. Zhu, Experimental investigation of CO₂ separation by adsorption methods in natural gas purification, *Appl. Energy* 179 (2016) 329–337, <https://doi.org/10.1016/j.apenergy.2016.06.146>.
- [11] D. Saha, Z. Bao, F. Jia, S. Deng, Adsorption of CO₂, CH₄, N₂ O, and N₂ on MOF-5, MOF-177, and Zeolite 5A, *Environ. Sci. Technol.* 44 (2010) 1820–1826, <https://doi.org/10.1021/es9032309>.
- [12] S. Cavenati, C.A. Grande, A.E. Rodrigues, Adsorption equilibrium of methane, carbon dioxide, and nitrogen on zeolite 13X at high pressures, *J. Chem. Eng. Data* 49 (2004) 1095–1101, <https://doi.org/10.1021/jc0498917>.
- [13] J.A.C. Silva, A.F. Cunha, K. Schumann, A.E. Rodrigues, Binary adsorption of CO₂/CH₄ in binderless beads of 13X zeolite, *Microporous Mesoporous Mater.* 187 (2014) 100–107, <https://doi.org/10.1016/j.micromeso.2013.12.017>.
- [14] P. Leflaive, G.D. Pirngruber, A. Faraj, P. Martin, G.V. Baron, J.F.M. Denayer, Statistical analysis and Partial Least Square regression as new tools for modelling and understanding the adsorption properties of zeolites, *Microporous Mesoporous Mater.* 132 (2010) 246–257, <https://doi.org/10.1016/j.micromeso.2010.03.004>.
- [15] A. Martín-Calvo, J.B. Parra, C.O. Ania, S. Calero, Insights on the anomalous adsorption of carbon dioxide in LTA zeolites, *J. Phys. Chem. C.* 118 (2014) 25460–25467, <https://doi.org/10.1021/jp507431c>.
- [16] E.J. García, J. Pérez-Pellitero, G.D. Pirngruber, C. Jallut, M. Palomino, F. Rey, S. Valencia, Tuning the adsorption properties of zeolites as adsorbents for CO₂ separation: best compromise between the working capacity and selectivity, *Ind. Eng. Chem. Res.* 53 (2014) 9860–9874, <https://doi.org/10.1021/ie500207s>.
- [17] F. Brandani, D.M. Ruthven, The effect of water on the adsorption of CO₂ and C₃H₈ on type X zeolites, *Ind. Eng. Chem. Res.* 43 (2004) 8339–8344, <https://doi.org/10.1021/ie040183o>.
- [18] Y. Wang, M.D. LeVan, Adsorption equilibrium of binary mixtures of carbon dioxide and water vapor on zeolites 5A and 13X, *J. Chem. Eng. Data* 55 (2010) 3189–3195, <https://doi.org/10.1021/je100053g>.
- [19] M. Palomino, A. Corma, F. Rey, S. Valencia, New insights on CO₂–methane separation using LTA zeolites with different Si/Al ratios and a first comparison with MOFs, *Langmuir* 26 (2010) 1910–1917, <https://doi.org/10.1021/la9026656>.
- [20] T.D. Pham, R.F. Lobo, Adsorption equilibria of CO₂ and small hydrocarbons in AEI-, CHA-, STT-, and RRO-type siliceous zeolites, *Microporous Mesoporous Mater.* 236 (2016) 100–108, <https://doi.org/10.1016/j.micromeso.2016.08.025>.

- [21] Z. Pourmahdi, H. Maghsoudi, Adsorption isotherms of carbon dioxide and methane on CHA-type zeolite synthesized in fluoride medium, *Adsorption* 23 (2017) 799–807, <https://doi.org/10.1007/s10450-017-9894-1>.
- [22] X. Su, P. Tian, D. Fan, Q. Xia, Y. Yang, S. Xu, L. Zhang, Y. Zhang, D. Wang, Z. Liu, Synthesis of DNL-6 with a high concentration of Si (4 Al) environments and its application in CO₂ separation, *ChemSusChem* 6 (2013) 911–918, <https://doi.org/10.1002/cssc.201200907>.
- [23] Z. Bacsik, O. Cheung, P. Vasiliev, N. Hedin, Selective separation of CO₂ and CH₄ for biogas upgrading on zeolite NaKA and SAPO-56, *Appl. Energy* 162 (2016) 613–621, <https://doi.org/10.1016/j.apenergy.2015.10.109>.
- [24] E. Pérez-Botella, R. Martínez-Franco, N. González-Camuñas, Á. Cantín, M. Palomino, M. Moliner, S. Valencia, F. Rey, Unusually Low Heat of Adsorption of CO₂ on ALPO and SAPO Molecular Sieves, *Front Chem.* 8 (2020) 1–10, <https://doi.org/10.3389/fchem.2020.588712>.
- [25] R. Kapoor, P. Ghosh, M. Kumar, V.K. Vijay, Evaluation of biogas upgrading technologies and future perspectives: a review, *Environ. Sci. Pollut. Res.* (2019), <https://doi.org/10.1007/s11356-019-04767-1>.
- [26] L. Grajciar, J. Čejka, A. Zukal, C. Otero Areán, G. Turnes Palomino, P. Nachtigall, Controlling the adsorption enthalpy of CO₂ in zeolites by framework topology and composition, *ChemSusChem* 5 (2012) 2011–2022, <https://doi.org/10.1002/cssc.201200270>.
- [27] E.J. García, J. Pérez-Pellitero, C. Jallut, G.D. Pirngruber, Quantification of the confinement effect in microporous materials, *Phys. Chem. Chem. Phys.* 15 (2013) 5648–5657, <https://doi.org/10.1039/c3cp44375b>.
- [28] J. Shang, G. Li, R. Singh, Q. Gu, K.M. Nairn, T.J. Bastow, N. Medhekar, C. M. Doherty, A.J. Hill, J.Z. Liu, P.A. Webley, Discriminative separation of gases by a “molecular trapdoor” mechanism in chabazite zeolites, *J. Am. Chem. Soc.* 134 (2012) 19246–19253, <https://doi.org/10.1021/ja309274y>.
- [29] M.M. Lozinska, J.P.S. Mowat, P.A. Wright, S.P. Thompson, J.L. Jorda, M. Palomino, S. Valencia, F. Rey, Cation gating and relocation during the highly selective “trapdoor” adsorption of CO₂ on univalent cation forms of zeolite Rho, *Chem. Mater.* 26 (2014) 2052–2061, <https://doi.org/10.1021/cm404028f>.
- [30] E.L. Bruce, V.M. Georgieva, M.C. Verbraeken, C.A. Murray, M.F. Hsieh, W. J. Casteel, A. Turrina, S. Brandani, P.A. Wright, Structural chemistry, flexibility, and CO₂ adsorption performance of alkali metal forms of merlinoite with a framework Si/Al ratio of 4.2, *J. Phys. Chem. C* 125 (2021) 27403–27419, <https://doi.org/10.1021/acs.jpcc.1c08296>.
- [31] M. Palomino, A. Corma, J.L. Jordá, F. Rey, S. Valencia, Zeolite Rho: a highly selective adsorbent for CO₂/CH₄ separation induced by a structural phase modification, *Chem. Commun. (Camb.)* 48 (2012) 215–217, <https://doi.org/10.1039/c1cc16320e>.
- [32] J.G. Min, K.C. Kemp, H. Lee, S.B. Hong, CO₂ adsorption in the RHO family of embedded isorecticular zeolites, *J. Phys. Chem. C* 122 (2018) 28815–28824, <https://doi.org/10.1021/acs.jpcc.8b09996>.
- [33] M. Feng, T. Andrews, E. Flores, *Hydrocarbon Processing - 2012 Gas Processes Handbook*, Gulf Publishing Company, 2012.
- [34] D. Xie, S.I. Zones, H. Huang, J.A. Thompson, H.S. Lacheen, C. Mathieux, Separation of gases using zeolite SSZ-45, US 8926735 B1, 2015.
- [35] E.W. Jr. Corcoran, A. Corma Canos, F. Rey Garcia, S. Valencia Valencia, A. Cantin Sanz, M. Palomino Roca, Separation, storage and catalytic conversion of fluids using ITQ-55, WO 2015/196023 A1, 2015.
- [36] P.A. Barrett, M.-J. Diaz-Cabañas, M.A. Cambor, Crystal structure of zeolite MCM-35 (MTF), *Chem. Mater.* 11 (1999) 2919–2927, <https://doi.org/10.1021/cm9910660>.
- [37] T. Boix, M. Puche, M.A. Cambor, A. Corma, Synthetic porous crystalline material ITQ-12, its synthesis and use, US 6471939 B1, 2002.
- [38] P.A. Barrett, T. Boix, M. Puche, D.H. Olson, E. Jordan, H. Koller, M.A. Cambor, ITQ-12: a new microporous silica polymorph potentially useful for light hydrocarbon separations, *Chem. Commun.* (2003) 2114, <https://doi.org/10.1039/b306440a>.
- [39] A. Cantín, A. Corma, S. Leiva, F. Rey, J. Rius, S. Valencia, Synthesis and structure of the bidimensional zeolite ITQ-32 with small and large pores, *J. Am. Chem. Soc.* 127 (2005) 11560–11561, <https://doi.org/10.1021/ja053040h>.
- [40] A. Corma, F. Rey, J. Rius, M.J. Sabater, S. Valencia, Supramolecular self-assembled molecules as organic directing agent for synthesis of zeolites, *Nature* 431 (2004) 287–290, <https://doi.org/10.1038/nature02909>.
- [41] M.-J. Díaz-Cabañas, P.A. Barrett, Synthesis and structure of pure SiO₂ chabazite: the SiO₂ polymorph with the lowest framework density, *Chem. Commun.* 29 (1998) 1881–1882, <https://doi.org/10.1039/a804800b>.
- [42] J.G. Moscoco, G.J. Lewis, J.L. Gisselquist, M.A. Miller, L.M. Rohde, Crystalline aluminosilicate zeolitic composition: UZM-9, WO 03068679 A1, 2003.
- [43] F.S.O. Ramos, E.C.O. Munsignatti, H.O. Pastore, 2D–3D structures: the hydrothermal transformation of a layered sodium silicate, Na-RUB-18, into mordenite zeolite, *Microporous Mesoporous Mater.* 177 (2013) 143–150, <https://doi.org/10.1016/j.micromeso.2013.04.017>.
- [44] F.S.O. Ramos, H.O. Pastore, 2D-to-disguised 3D materials with built-in acid sites: H + [Al]-RUB-18, *Dalton Trans.* 46 (2017) 11728–11737, <https://doi.org/10.1039/c7dt02241g>.
- [45] Y. Asakura, S. Osada, N. Hosaka, T. Terasawa, K. Kuroda, Optimal topotactic conversion of layered octosilicate to RWR-type zeolite by separating the formation stages of interlayer condensation and elimination of organic guest molecules, *Dalton Trans.* 43 (2014) 10392–10395, <https://doi.org/10.1039/C3DT53533A>.
- [46] L. Mafra, J.A. Vidal-Moya, T. Blasco, Structural characterization of zeolites by advanced solid state NMR spectroscopic, *Methods* (2012), <https://doi.org/10.1016/B978-0-12-397020-6.00004-0>.
- [47] M. Thommes, K. Kaneko, A.V. Neimark, J.P. Olivier, F. Rodriguez-Reinoso, J. Rouquerol, K.S.W. Sing, Physisorption of gases, with special reference to the evaluation of surface area and pore size distribution (IUPAC technical report), *Pure Appl. Chem.* 87 (2015) 1051–1069, <https://doi.org/10.1515/pac-2014-1117>.
- [48] M.M. Dubinin, Physical adsorption of gases and vapors in micropores, in: D. A. Cadenhead, J.F. Danielli, M.D. Rosenberg (Eds.), *Progress in Surface and Membrane Science*, Elsevier, 1975, pp. 1–70, <https://doi.org/10.1016/B978-0-12-571809-7.50006-1>.
- [49] K. Kawazoe, G. Horváth, Method for the calculation of effective pore size distribution in molecular sieve carbon, *J. Chem. Eng. Jpn.* 16 (1983) 470–475.
- [50] A.L. Myers, J.M. Prausnitz, Thermodynamics of mixed-gas adsorption, *Am. Inst. Chem. Eng. J.* 11 (1965) 121–127, <https://doi.org/10.1002/aic.690110125>.
- [51] C.M. Simon, B. Smit, M. Haracznyk, PyIAST: ideal adsorbed solution theory (IAST) python package, *Comput. Phys. Commun.* 200 (2016) 364–380, <https://doi.org/10.1016/j.cpc.2015.11.016>.
- [52] A. Malek, S. Farooq, Determination of equilibrium isotherms using dynamic column breakthrough and constant flow equilibrium desorption, *J. Chem. Eng. Data* 41 (1996) 25–32, <https://doi.org/10.1021/je950178e>.
- [53] R.T. Yang, Gas Separation by Adsorption Processes, 1987. <https://doi.org/10.1016/B978-0-409-90004-0.50013-1>.
- [54] M.M. Foss, Interstate Natural Gas — Quality Specifications & Interchangeability, Sugar Land, TX, 2004.
- [55] G. Sastre, A. Corma, The confinement effect in zeolites, *J. Mol. Catal. A Chem.* 305 (2009) 3–7, <https://doi.org/10.1016/j.molcata.2008.10.042>.
- [56] T.D. Pham, R. Xiong, S.I. Sandler, R.F. Lobo, Experimental and computational studies on the adsorption of CO₂ and N₂ on pure silica zeolites, *Microporous Mesoporous Mater.* 185 (2014) 157–166, <https://doi.org/10.1016/j.micromeso.2013.10.030>.
- [57] N.S. Wilkins, A. Rajendran, S. Farooq, Dynamic column breakthrough experiments for measurement of adsorption equilibrium and kinetics, *Adsorption* 27 (2021) 397–422, <https://doi.org/10.1007/s10450-020-00269-6>.
- [58] G. Cao, M.J. Shah, S.C. Reyes, Synthesis of ITQ-12, US 2008/0107594 A1, 2008.
- [59] Q. Wu, X. Liu, L. Zhu, X. Meng, F. Deng, F. Fan, Z. Feng, C. Li, S. Maurer, M. Feyen, U. Müller, F.S. Xiao, Solvent-free synthesis of ITQ-12, ITQ-13, and ITQ-17 zeolites, *Chin. J. Chem.* 35 (2017) 572–576, <https://doi.org/10.1002/cjoc.201600646>.